JMEPEG (2006) 15:505-518
DOI: 10.1361/105994906X136070

1059-9495/$19.00

Numerical Analysis of Friction Stir Welding Process

R.K. Uyyuru and Satish V. Kailas

(Submitted August 12, 2005; in revised form December 30, 2005)

Friction stir welding (FSW), which has several advantages over the conventional welding processes, is a solid-state welding process where no gross melting of the material being welded takes place. Despite significant advances over the last decade, the fundamental knowledge of thermomechanical processes during FSW is still not completely understood. To gain physical insight into the FSW process and the evaluation of the critical parameters, the development of models and simulation techniques is a necessity. In this article, the available literature on modeling of FSW has been reviewed followed by details of an attempt to understand the interaction between process parameters from a simulation study, performed using commercially available nonlinear finite element (FE) code DEFORM. The distributions of temperature, residual stress, strain, and strain rates were analyzed across various regions of the weld apart from material flow as a means of evaluating process efficiency and the quality of the weld. The distribution of process parameters is of importance in the prediction of the occurrence of welding defects, and to locate areas of concern for the metallurgist. The suitability of this modeling tool to simulate the FSW process has been discussed. The lack of the detailed material constitutive information and other thermal and physical properties at conditions such as very high strain rates and elevated temperatures seems to be the limiting factor while modeling the FSW process.

Keywords FE-simulation, friction stir welding (FSW), numerical analysis

1. Introduction

The friction stir welding (FSW) process has taken many giant steps forward and has found many applications since its invention at TWI (The Welding Institute, Cambridge, UK) in 1991. Substantial development of FSW has been reported subsequently, where FSW has been used, especially, to produce high-quality joints in Al alloys (Ref 1-19). Many alloys, including most aerospace Al alloys (e.g., Al 7xxx) and those regarded as difficult to weld by fusion processes (e.g., Al 2xxx), may be welded by FSW (Ref 1-3, 20-25). It allows continuous butt and lap joints to be made in metals including Al, Pb, Mg, Ti, Cu, Zn, steel, and metal matrix composites. During FSW, the weld is made in the solid phase (i.e., no gross melting of the material being welded takes place). It is a process that utilizes local friction heating to produce continuous solid-state seams. The solid-state, low-distortion welds produced during FSW are achieved with relatively low cost using simple and energy-efficient mechanical equipment. Conventional FSW is a maturing process that is currently used in the maritime, automotive, and aerospace fabrication industries.

Figure 1 presents a schematic view of FSW. A specially designed cylindrical tool, made from a hard and wear-resistant material relative to the material being welded, with a profiled pin is rotated and plunged into the abutting edges of the plates to be joined. The height of the pin will be just short of the thickness of plates to be welded so that during the plunging, the shoulder of the tool comes in contact with the plate surface before the pin penetrates through the plates. The plates have to be clamped onto a backing bar in a manner that prevents the abutting joint faces from being forced apart. After entry of the profiled pin to almost the thickness of the material and to allow the tool shoulder to just penetrate into the plate, the rotating tool will translate along the joint line. Frictional heat generated between the wear-resistant welding tool and the material of the plates causes the latter to soften without reaching the melting point and allows traversing of the tool along the weld line. The plasticized material is transferred from the leading edge of the tool to the trailing edge of the tool, where it cools and consolidates to produce a high-integrity weld in the solid phase. Thus, the process involves relatively high temperatures and very high strain rates. The plasticized material will get forged by the intimate contact with the tool shoulder and the pin profile during this process.

The process includes advantages like high-strength welds, low distortion, no need for filler material, no need of postweld treatments, and immunity toward defects and property deterio-

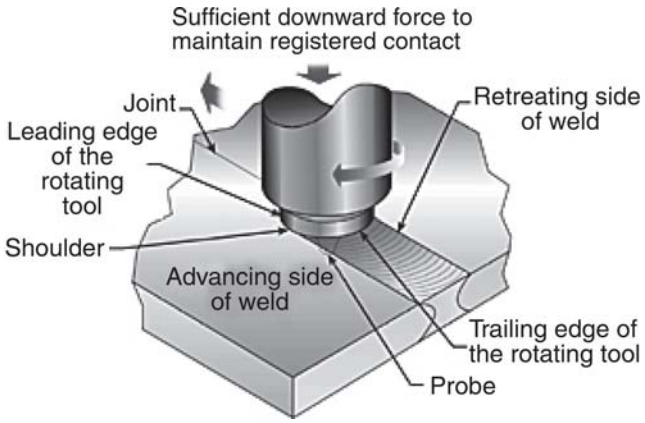

Fig. 1 Schematic presentation of the FSW process (Ref 26)

R.K. Uyyuru and **Satish V. Kailas,** Department of Mechanical Engineering, Indian Institute of Science, Bangalore 560 012, India. Contact e-mail: uyyuru@yahoo.com.

ration associated with the solidification process in fusion welding. These advantages are attributed to the fact that the FSW process takes place in the solid phase below the melting point of the materials to be joined. Other advantages include a highly repeatable weld process with low defect rates and reduced safety concerns due to the elimination of weld fumes.

However, due to the complicated interaction between the tool and workpieces, and the typical squeezing type of material flow, there exist unavoidable limitations to the application of the process. The main limitations and areas for further research of the FSW process can be summarized as follows:

- Welding speeds are somewhat slower than those of some fusion welding processes.
- Workpieces need to be rigidly clamped.
- Support is required on opposite sides of workpieces.
- There is a keyhole at the end of each weld seam.
- Residual stresses develop.
- It is difficult to understand tool material/workpiece material interactions.
- The modeling of material flow and thermomechanical modeling.
- Tool material development to extend the technology to materials with high melting point.
- The evolution of microstructure and properties of friction stir welded joints.

The self-reacting FSW process eliminates or minimizes some of the disadvantages by providing a bottom shoulder in place of an anvil. These improvements include the reduction of process loads and an increase in welding speed. The weld head uses two shoulders that interface with the top and bottom surfaces of the workpieces being joined. These top and bottom shoulders are independently actuated and biased to follow the profile of a workpiece and supply a balanced load to the opposed surfaces of the workpiece during the welding operation (Ref 27).

The goal of manufacturing research and development is to determine the optimum means of producing sound products. The optimization criteria may vary depending on product requirements, but establishing an appropriate criterion requires a thorough understanding of the mechanics involved in that particular manufacturing process. Without the knowledge of the influences of variables such as friction conditions, material properties, and workpiece-and-tool geometry on the process mechanics, it would not be possible to design the equipment adequately, or to predict and prevent the occurrence of defects. Thus, process modeling by computer simulation has been a major concern in modern manufacturing technology to assist in finding the optimization criteria.

Process modeling can enable the user to predict when and by how much the properties of a system will change. It involves the modeling of physical processes with the aim of studying interactions between different process parameters and their distribution, resulting in the alternation of physical and mechanical properties of the product. This capability can bring many benefits such as increased product quality, a better understanding of physical insight, and improved process design. In short, an improved understanding of the process can be gained. Computer software models are good at examining these interactions, which are often too complex for people to comprehend or predict even though real-life experimentation is used. FSW process modeling can be performed for a better understanding, and thus an improvement, of the process.

Fundamental, science-based modeling and understanding of the FSW process can greatly reduce the cost and cycle time of its application in joining operations. Accurate modeling of the FSW process will enable the rapid development of the process, in particular with regard to tool design. However, this type of simulation requires a three-dimensional (3-D), fully coupled, thermomechanical, solid-based model with associated high computational cost. Model predictions are crucial to be able to follow the complex evolution of material deformation and microstructure. The deformation and flow patterns are important in avoiding voids and weld defects in FSW design. Tracking the changes in microstructure is necessary for the optimization of the mechanical and corrosion properties of the welds, which in turn are intimately linked to the evolved microstructures. Local thermomechanical cycles, which are imposed through the combination of frictional heating and mechanical working by the tool, are believed to be causing microstructural evolution in FSW-processed alloys. The heat generation is closely related to the friction condition at the contact interface between the FSW tool and the workpiece materials as well as the material flow in the weld matrix, because the mechanisms for heat generation by frictional and plastic dissipation are different. The heat generation from the tool is governed by the contact condition (i.e., whether there is sliding, sticking, or partial sliding/sticking). The contact condition in FSW is very complex, and is dependent on the alloy, welding parameters, and tool design.

2. Relation to and Summary of Relevant Literature

Although considerable experimental work has been reported in the published literature, modeling work of the FSW process appears to be very scarce. In an effort to understand the complex nature of the process and for development of the process, modeling of the process seems to be the key route to progress. The sole purpose of the modeling is to quantify the interaction between different process parameters with an aim to understanding the intricate nature of the process. The resultant trends of the process parameters from modeling work can be compared with experimental results and thus are useful in optimizing the welding conditions. The following section details the available modeling efforts of FSW. Because little is known about the physics involved during the FSW process, the objective here is to further improve the understanding of the process through numerical modeling.

2.1 Thermomechanical Modeling

There has been considerable effort in modeling FSW to optimize the thermomechanical conditions. Chen and Kovacevic (Ref 28, 29) used a commercially available FE-package, ANSYS (Canonsburg, PA), to perform 3-D FSW simulations for studying thermal impact, and the evolution of longitudinal, lateral, and vertical stresses in the weld by considering the mechanical effect of the tool. The authors have accomplished this by parametrically studying the effects of varying the welding parameters, primarily the traverse speed of the tool. It was found that the maximum temperature gradients in longitudinal and lateral directions are located just beyond the shoulder edge, and also that the longitudinal residual stress is greater than the lateral residual stress at the top surface of the weld. A higher traverse speed was found to induce a larger high

longitudinal stress zone and a narrower lateral stress zone in the weld.

Song and colleagues (Ref 30-32) proposed a heat-transfer model to describe the detailed 3-D transient heat-transfer process for predicting temperatures in FSW. The material latent heat was also considered in the model for modeling possible phase changes in the welding. An explicit central differential scheme has been used in solving the control equations, which were developed using FORTRAN. There have been many noticeable efforts of numerical modeling for predicting heat generation and consequent temperature effects in FSW (Ref 33-35).

An FE-based 3-D thermal model of the FSW process has been presented by Khandkar et al. (Ref 36-38) to predict the temperature distribution and the residual stresses caused by the thermal cycles during FSW. Reasonably good correlation between the simulated temperature profiles and experimental data has been observed. In this study, a combined modeling and experimental approach has been used in an attempt to develop a practical predictive tool for the distribution of residual stresses. The model appears to have captured the asymmetry of the process, but the peak residual strain is considerably higher than the measured values (Ref 39). In an effort to predict the distribution of residual stresses, two different numerical modeling tools were used, and the results were mutually compared for greater efficiency by Lawrjaniec et al. (Ref 40). In another interesting modeling effort, the effects of process parameters, such as thermal diffusivity and viscosity, on the trends in axial forces, required torques, and potential weld defect formation are studied using the computational fluid dynamics concept (Ref 41).

As mentioned in earlier sections, thermomechanical effects are believed to cause microstructural changes during FSW. Heutier et al. (Ref 42) tried to highlight the development of the characteristic microstructures generated based on a thermomechanical simulation of the FSW process. The analytical results were complemented by FE-calculated velocity fields while describing the vertical flow of material subjected to the weld (Ref 42). Reynolds et al. (Ref 43) presented an experimental correlation of weld efficiency and defect formation by using a two-dimensional (2-D) FSW model based on Eulerian flow formulation. A specific weld energy comparison for a range of welding speeds and tool rotation rates shows that the effect of weld pitch on specific weld energy was much less than that of welding speed, and the weld energy appeared to approach some minimum value, independent of pitch, as the welding speed was increased (Ref 43). Schmidt et al. (Ref 44) studied the material-tool interface contact condition and the subsequent heat generation during the weld process by developing an analytical model combined with a Eulerian FE analysis of the temperature field. The heat generation was closely related to the friction condition at the contact interface between the FSW tool and the weldpiece material as well as the material flow in the weld matrix, because the mechanisms for heat generation by frictional and plastic deformation are different. The heat generation from the tool was governed by the contact condition (i.e., whether there is sliding, sticking, or partial sliding/sticking). A combination of Coulomb's law of friction for the sliding condition and the material yield shear stress for the sticking condition to model the contact forces were used in their model, thus enabling a contact condition, which could be partial sliding/sticking. Analytical results were combined with experimental results to deduce which contact condition is most likely to be present during welding. A 3-D analysis developed by Askari et al. (Ref 45) captured the coupling among tool geometry, heat generation, and plastic flow of the material under complex asymmetric thermomechanical loading conditions. Thus, this model was useful in predicting the deformation and flow patterns that are important in avoiding voids and weld defects in FSW design (Ref 45).

Numerical models could be useful in designing welding tools that can yield desired thermal gradients in view of avoiding tool breakage. In his work, Ulysse (Ref 46) demonstrated the development of a 3-D visco-plastic model for the FSW process using the commercial software FIDAP. Parametric studies have been conducted on butt joints for aluminum thick plates to determine the effect of tool speeds on plate temperatures and to validate the model predictions with available measurements. It was also found that pin forces increase with increasing welding speeds, but the opposite effect has been observed for increasing rotational speeds.

Good agreement between predicted results and experimental neutron diffraction results of residual stresses in FSW was achieved by Zhu and Chao (Ref 47) using an in-house built 3-D elastic-plastic thermomechanical finite-element code (WELDSIM). The code was also used to study the effect of fixture release on the residual stresses after the welding process. It is important to consider residual stresses because the FSW process involves the application of pressures through fixtures.

Some limitations of numerical tools were put forward by Aramayo et al. (Ref 48) while using LS-DYNA, a commercial FE tool for modeling the flow field in the workpiece in the vicinity of the tool. Two different approaches, arbitrary Eulerian Lagrangian and computational fluid dynamics, were used, but it was found that there are limitations in terms of coupling the flow fields with the temperature fields generated by friction, and in using material models that incorporate the temperature-dependent stress-strain-strain rate and viscosity effects (Ref 48).

In another instance of discrepancy between the measured and predicted loads, Lockwood et al. (Ref 49) in their article examined the global and local mechanical response of friction stir-welded AA2024 alloy both experimentally and numerically. Full field strain measurements were obtained on transversely loaded tensile specimens via the digital image correlation technique. Assuming an iso-stress configuration, local constitutive data were determined for the various weld regions and used as input for a 2-D finite-element model. All analyses were performed on a personal computer using the ABAQUS (Providence, RI) software package. It was found that the most likely reason for the results was the iso-stress assumption for the heterogeneous weld (Ref 49). Later, the assumptions were refined and further verified. It was found that nearly plane stress conditions existed in the specimen as demonstrated by the correspondence between experimental results and the predictions of the 2-D models (Ref 50).

DEFORM (Columbus, OH), a commercial FE package, was used by Buffa and Fratini (Ref 51) and Fratini and Buffa (Ref 52) to highlight the material flux, temperature, strain, strain rate distributions, and recrystallization during the FSW process. The process mechanics of a linear butt joint of AA6082-T6 sheets was investigated. In addition, material microstructure evolution due to recrystallization phenomena was also accounted for. They concluded that DEFORM was capable of emerging as a design tool for FSW if the tool could be im-

proved, in the sense that it should incorporate details like friction into the analysis technique more precisely.

2.2 Flow Modeling

The modeling of FSW has largely concentrated on the simulation of temperature evolution and residual stresses (i.e., on developing the tools and procedures for making reliable welds and on characterizing the properties of the welds), as explained in an earlier section. The main limitation is that these simulations are a posteriori simulations, which generally do not model the material flow or the generation of heat due to friction or plastic deformation. Instead, they rely on the measurement of data such as heat input during FSW experiments as input parameters for the simulations. Unfortunately, very little is known about the material flow behavior during FSW from numerical simulations. It is perceived that a process model could yield more information on material mixing, defect presence, and retained oxide films. Available material flow simulation results, which are mostly experiment-oriented, are summarized in the following paragraphs.

Under varying welding conditions, the material flow and microstructural evolution in the friction stir welds of a 6061-Al alloy to itself and of a 6061-Al alloy to 2024-Al alloy plates were studied by Ouyang and Kovacevic (Ref 53). The results showed that plastic deformation, flow, and mechanical mixing of the material exhibit distinct asymmetric characteristics on either side of both similar and dissimilar welds. Based on the measured results in the welds of the 6061-Al alloy, the material movement within welds is considered to be, by either simple extrusion or chaotic mixing, dependent on where the material originates within the weld zone. Encouraging evidence for stirring action was detected in the weld zone. Guerra et al. (Ref 54) also observed in their experiments that flow on the advancing side is different from that on the retreating side of the weld while developing the rotational model of material movement. Different thermomechanical histories and properties were also observed on either side on the welds. Moreover, it was found that material near the top of the weld moves under the influence of the shoulder rather than the threads on the pin.

Murr et al. (Ref 55-58) used differential etching of Al alloys in a study of complex residual, intercalated, lamellar-like flow patterns while developing a mechanistic view of the FSW process based on dynamic recrystallization, accommodating extreme solid-state plastic flow. The intercalated microstructures were found to be dominated by dynamic recrystallization. The flow patterns were observed to be complex spirals and vortex-like shapes, among others, and they changed somewhat systematically with tool rotation speeds between 400 and 1200 rotations per minute (rpm), depending on tool orientation. The FSW process was characterized by extreme plastic deformation in the solid state; there is no associated melting. Reynolds (Ref 59) applied the same concept of differential etching by using the marker material for a qualitative understanding of material flow, resulting in the development of a reasonable physical interpretation of the working of the FSW process: an interpretation devoid of conjecture resulting from possibly faulty intuition. This qualitative understanding of material flow has been complimented by quantitative weld metallography, which had shown that tool geometry, at least over a limited range of variation, could produce changes in stir weld microstructure, but the broad features of the weld microstructure are constant.

A unique concept of flow visualization during FSW was due to Colligan (Ref 60), who expended steel balls as tracers that were embedded in weld path to gain insight into the movement of material during FSW. A stop-action technique was implemented where the process was stopped at specific intervals, and the position of the tracers was radiographed as an indirect means of determining material movement for the purpose. Based on quantitative results, it was concluded that material movement within friction stir welds has been accomplished by either simple extrusion or chaotic mixing, depending on where within the weld zone the material was originating. It was also observed that in friction stir welds not all material influenced by the pin was actually stirred in the welding process. Much of the material movement has been taking place by simple extrusion. The material that was stirred originates from the upper portion of the path of the welding tool pin. These results can be handy in hypothesizing an empirical model for the FSW process.

The prominent surface feature of most friction stir welds has been the presence of onion rings. Krishnan (Ref 61) concluded that the origin of onion rings is nothing but a geometric effect caused by the fact that cylindrical sheets of material were extruded during each rotation of the tool and that the cutting through the section of the material produces an apparent onion ring.

The FSW has been described in terms of five conventional metal working zones: preheat; initial deformation; extrusion; forging; and post-heat/cool down (Ref 62). Using this approach and by considering mass balance, it is possible to attain a relationship among pin tool geometry, operating parameters, and the flow stress of the materials. Analysis of the extrusion zone flow also provides for the calculation of the width of the extrusion zone, strain rates, and x-direction pressure. Based on this analysis, which can be coupled with empirically determined relationships among processing parameters, maximum temperature, and material constitutive properties, an understanding of the conditions necessary to produce an "optimum" weld may emerge.

As explained in earlier sections, numerical modeling was very useful in thermomechanical modeling, which controls the microstructure evolution during the FSW. However, for a complete understanding of the process efficiency, material flow needs to be well understood. It was observed that material flow was mostly modeled by physical means rather than numerical means. It could be there might be certain limitations while modeling material flow numerically. Additional advantages like the prediction of sites for possible defects could be guaranteed, and, if it is possible to simulate the material flow numerically, a more complete understanding of the FSW process can be achieved. The objective of the current study, thus, was to model the material flow in FSW using an available metal-forming numerical tool, DEFORM.

3. Numerical Analysis

Process simulation of FSW was performed using the commercially available nonlinear finite-element code, DEFORM. It is an engineering software that enables designers to analyze metal-forming processes on the computer rather than on the shop floor using trial and error. Today's competitive pressures require companies to take advantage of every tool at their disposal. DEFORM has proven itself to be extremely effective in a wide range of research and industrial applications (Ref 63).

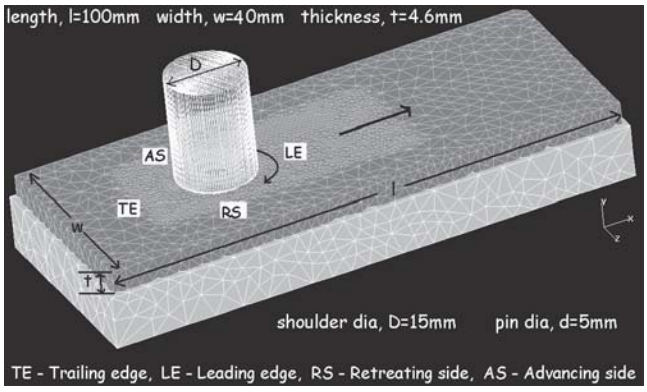

Fig. 2 Setup of FSW for numerical simulations

In this study, the tool (the probe and pin shoulder) was modeled as a rigid body, while the plate (the workpiece in shape of a plate) was modeled as a plastic body. It is to be observed that to avoid contact instabilities, only one plate was used in modeling the process. Material parameters were obtained from the database library of DEFORM. For ease of the operations, the probe (pin) was assumed to have a simple cylindrical shape with aspect ratio close to *one* and the edges were rounded by Φ 0.5 mm, which is not uncommon in real-life experiments. The tool was assumed to rotate at 1000 rpm, while it was allowed to transverse along the weld line at 1 mm/s. Thus, process conditions were assumed such that they were close to actual experiments. About 90% of the plastic deformation energy is assumed to be converted into heat. Interface friction conditions were modeled using the Coulomb coefficient of friction, which is equivalent to 0.7. Other experimental parameters are shown in Fig. 2. It was assumed that the process reached steady state once the probe traveled a minimum distance equal to its diameter. The workpiece was sectioned at many strategic locations perpendicular to the three principle axes for the purpose of revealing the distribution of process parameters along with the extent of material flow.

4. Simulation Results

Numerical simulations were analyzed for an understanding of the critical parameters and their distribution during the FSW. All results were analyzed at an instance of pin travel, represented by a pin travel distance of 6 mm (6000th step). This value was selected such that steady-state conditions might have prevailed as the pin moves into the material leaving the initial hole behind.

Distributions of different parameters are discussed in the following sections. The distribution of a particular parameter was analyzed over different cross sections (e.g., XY-plane, XZ-plane, and YZ-plane) while moving perpendicular to that particular cross section. The "shaded counters" option of DEFORM-3D was used to visualize the results at all cross sections. It is to be noted that origin of the coordinate axis lie at the plate center on the bottom surface.

4.1 Distribution of Temperatures (Range 25 to 325 °C)

4.1.1 Over XY-Plane (Sectioned Perpendicular to the Width of Plate). As depicted in Fig. 3, temperatures are

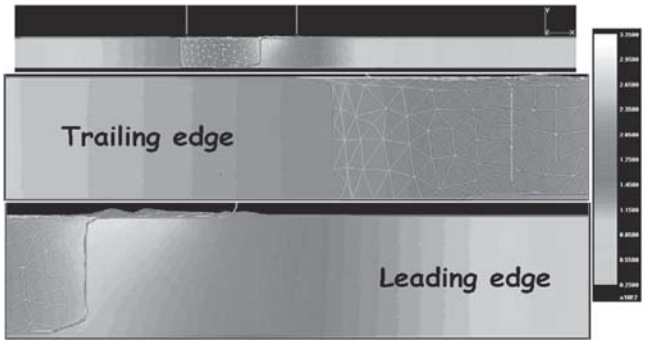

Fig. 3 Temperature distribution over the XY-plane

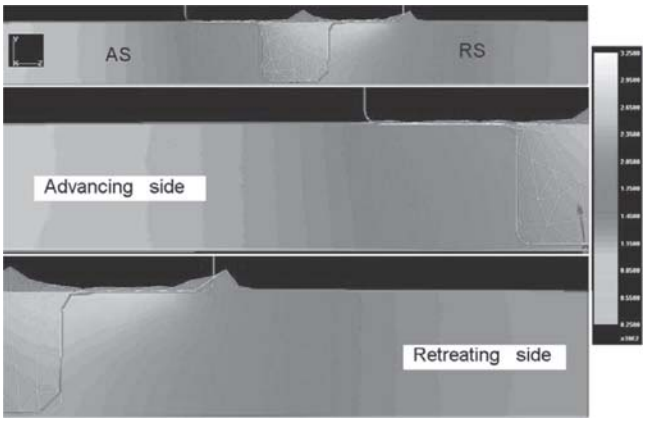

Fig. 4 Temperature distribution over the YZ-plane

>325 °C in the vicinity of the interface between tool and plate toward the leading edge. It was also observed from the figure that temperature gradients are higher toward the leading edge than toward the trailing edge. This discrepancy in temperature gradients can be attributed to the fact that near the leading edge new material will heat up while heated material will cool at the trailing edge. It was also observed that temperature gradients are less intense (i.e., higher temperatures are spread over longer distances toward the retreating side than that on the advancing side).

4.1.2 Over YZ-Plane (Sectioned Perpendicular to the Length of the Plate). As depicted by Fig. 4, temperatures are higher near the interface between the shoulder and the plate. It is to be observed from Fig. 4 that temperatures are widely distributed toward the retreating side of the tool than on the advancing side. It was also observed that temperature gradients are higher on the leading edge side than toward the trailing edge side. This distinction might probably be due to the mechanical working of the plate material where it gets compressed and/or extruded on the advancing side, whereas on the retreating side material will be sheared.

4.1.3 Over XZ-Plane (Section Perpendicular to the Plate Thickness). As can be observed from Fig. 5, temperatures are distributed over a large area as heat conduction must be taking place during the process. However, this is concentrated at the contact interfaces between the tool and the plate. It was also observed from Fig. 5 that the temperature profile has not changed considerably from the top of the plate toward the bottom surface. This might be due to either the small thickness (4.6 mm) and/or the high conductivity of the plate material.

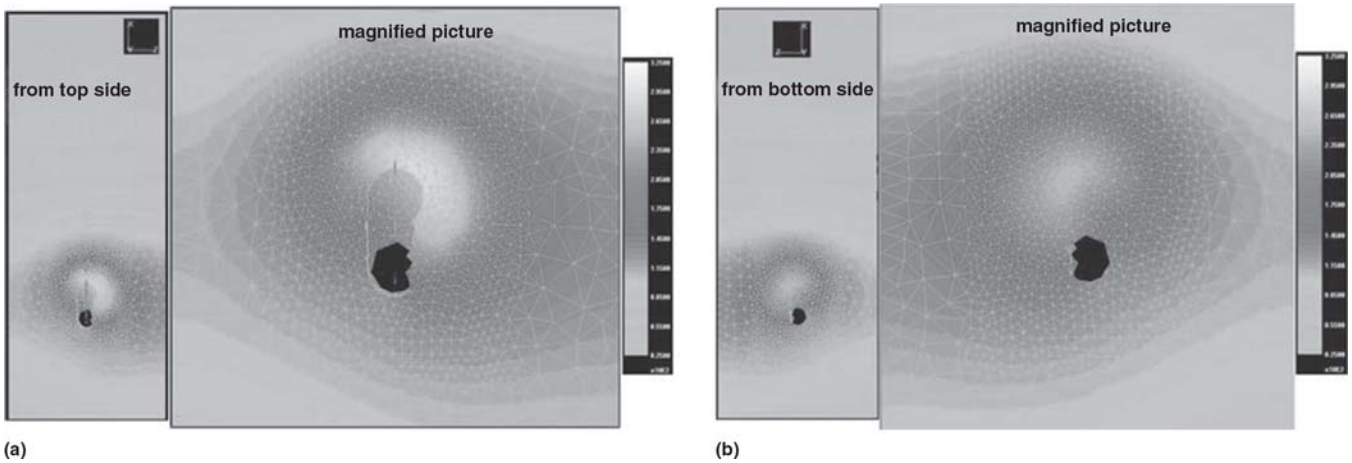

Fig. 5 Temperature distribution over the XZ-plane at the (a) top surface and (b) bottom surface

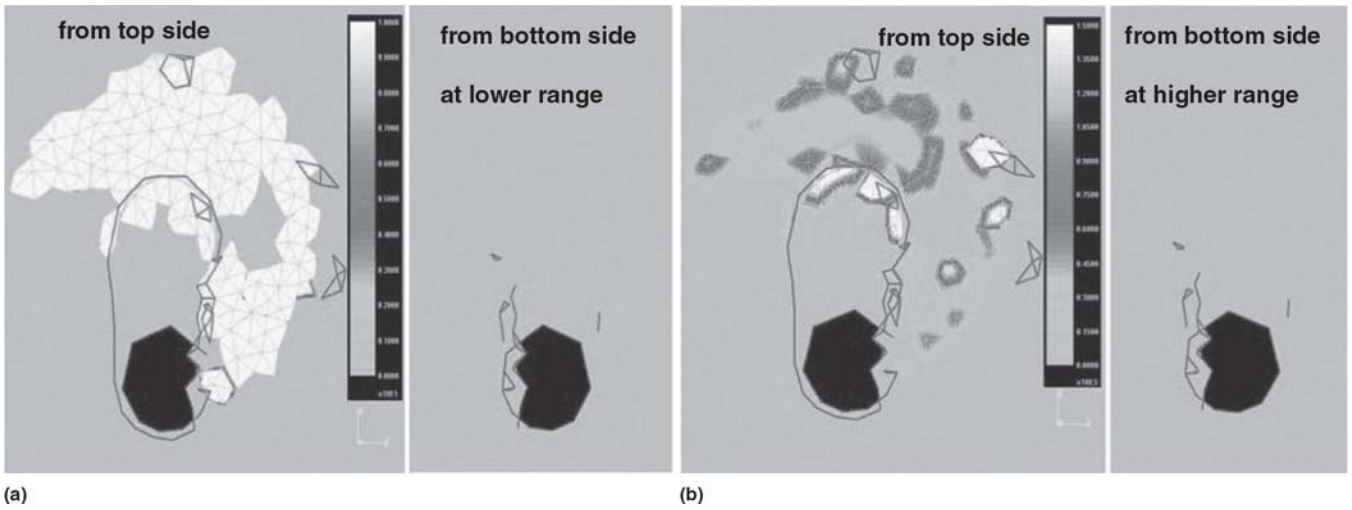

Fig. 6 Distribution of normal loads on the (a) top surface and (b) bottom surface of the plate

4.2 Distribution of Normal Loads

As shown in Fig. 6, normal loads are present all over the contact area between the plate and the tool shoulder. The variation of these loads might be due to the movement of elements in the thickness direction. It was observed that no normal loads exist on the bottom surface of the plate. The distributions of loads at two quantitative ranges are presented for the ease of distinction at low values and at high values. Distribution at low range shows a clear picture of normal loads, while distribution at the higher range represents the gradient across the surface. Load concentration areas shown in the right half of Fig. 5 might be due to element movement in a direction perpendicular to the plate surface.

4.3 Distribution of Effective Stresses (Range 100 to 300 MPa)

4.3.1 Over XY-Plane. As depicted by Fig. 7, the effective stress was varied across the width direction (z-axis) of the plate. The intensity of the effective stresses is comparatively low at the advancing side (Fig. 7a) than toward the retreating side (Fig. 7b). It can also be observed that the effective stresses are more intense and that their gradient is lower toward the retreating side.

4.3.2 Over YZ-Plane. Figure 8 presents the corresponding results of the distribution of effective stresses across the length direction of the plate. It was observed that the distribution of effective stresses toward the trailing edge (Fig. 8a), and the leading edge (Fig. 8b), are not much different. In both cases, low effective stresses are observed at a distance from the pin surface toward the retreating side of the pin.

4.3.3 Over XZ-Plane. As shown in Fig. 9 for the top surface of the plate (Fig. 9a) and for the bottom surface of the plate (Fig. 9b), the distributions of the effective stresses are quite predictable. It was observed that no significant variation of effective stress was found from the top surface of the plate to the bottom surface of the plate.

4.4 Distribution of the Mean Stresses (Range –300 to +300 MPa)

4.4.1 Over XY-Plane. As depicted in Fig. 10, the mean stresses are more intense and are distributed more widely toward the retreating side of the pin (Fig. 10b) than toward the advancing side (Fig. 10a). It was observed that the mean stresses are principally compressive in nature, but tensile mean stresses were observed in the vicinity of the contact interface between the pin and plate material. This may be because material was sheared on the retreating side before moving toward the advancing side.

4.4.2 Over YZ-Plane. As shown in Fig. 11, the mean

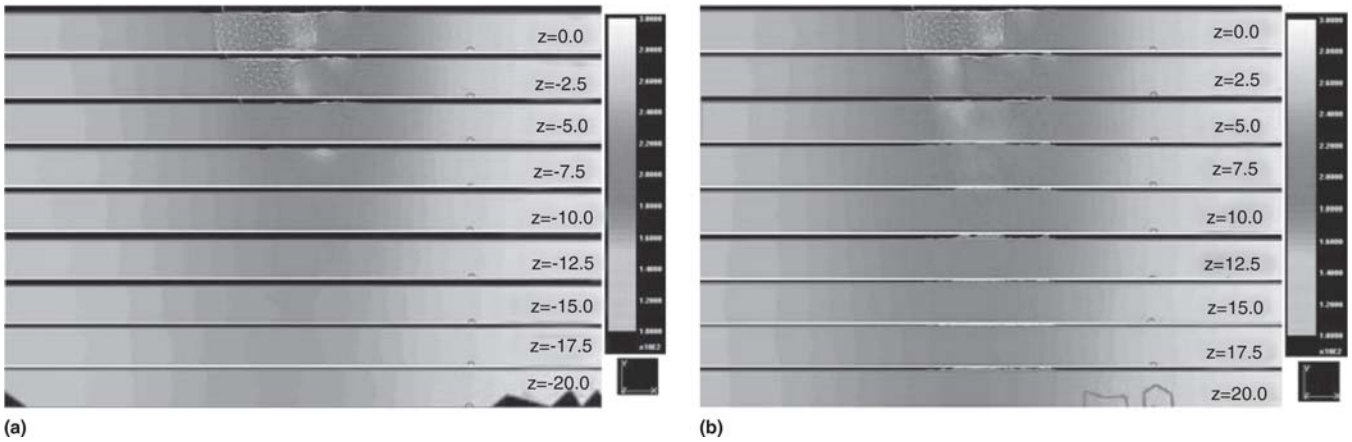

Fig. 7 Distribution of the effective stresses over the XY-plane

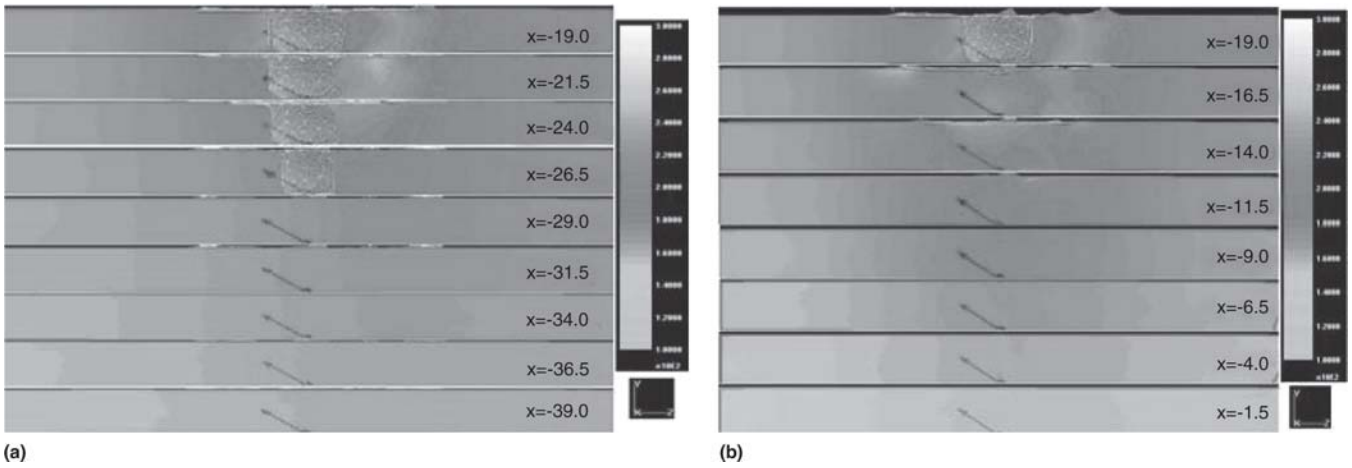

Fig. 8 Distribution of the effective stresses over the YZ-plane

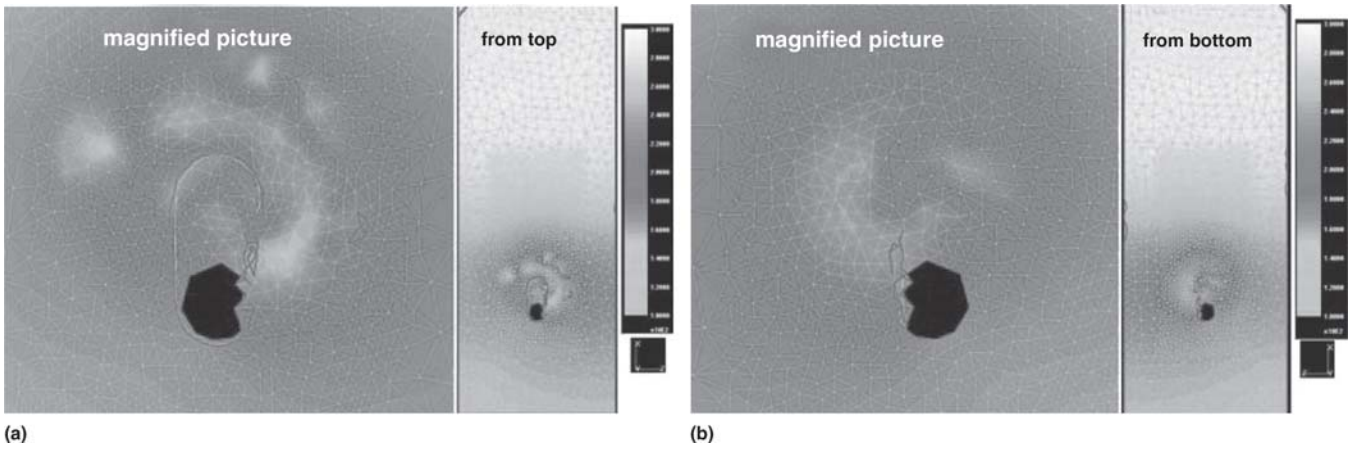

Fig. 9 Distribution of the effective stress over the (a) top surface and (b) bottom surface of the plate

stresses are again mostly negative (i.e., compressive in nature). It was observed that the distribution of mean stress is limited on the trailing edge side (Fig. 11a) but is widely distributed in front of the pin (Fig. 11b). As can be observed from Fig. 11, the presence of the tensile mean stresses on the advancing side of the weld line can lead to the occurrence of welding defects. Figure 12 shows the presence of a welding defect (crack) on the advancing side of the weld line from the experiments. Thus, it can be stated that DEFORM could reasonably simulate the welding process.

4.4.3 Over XZ-Plane. The distribution of the mean stresses in the through-thickness direction was quite the same, as shown in Fig. 13(a) (top side) and Fig. 13(b) (bottom side). It could have been due to the small thickness of the plate. It was

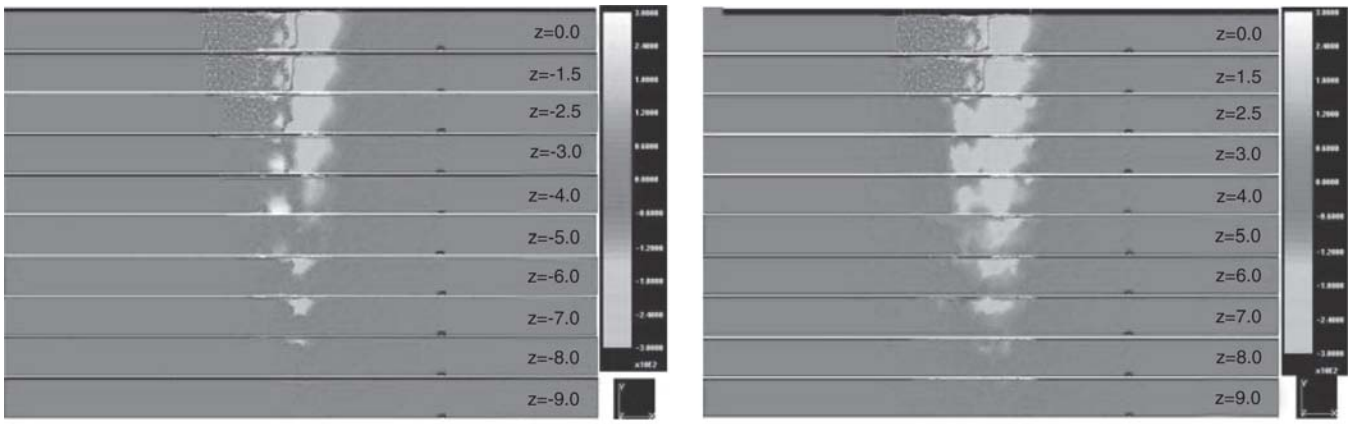

Fig. 10 Distribution of the mean stresses over the XY-plane toward the (a) advancing and (b) retreating sides

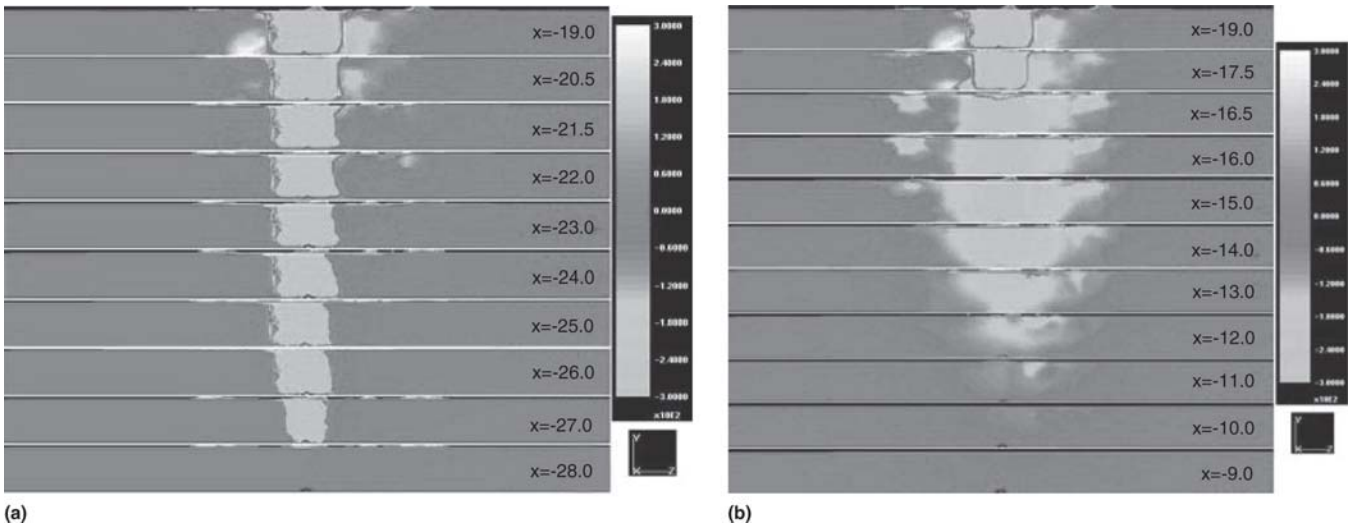

Fig. 11 Distribution of the mean stresses over the YZ-plane toward the (a) trailing and (b) leading edge sides

observed from both panels of Fig. 13 that there exists an area close to the edge of the tool shoulder where tensile mean stresses were present. These may again cause defects like surface cracks.

4.5 Distribution of Effective Strains (Range −10 to +10 mm/mm)

4.5.1 Over XY-Plane. As shown in Fig. 14, the effective strains are somewhat higher and more widely distributed toward the retreating side of the pin (Fig. 14a) than toward the advancing side of the pin (Fig. 14b). It was also observed that the effective strains were mostly concentrated around the pin interface with the plate material. This trend is predictable as plate material was replaced from the advancing side toward the retreating side.

4.5.2 Over YZ-Plane. Figure 15 represents the corresponding results of the distribution of effective strains over the YZ-plane. From Fig. 15, it was observed again that all strains were concentrated over the interface between the pin and plate material.

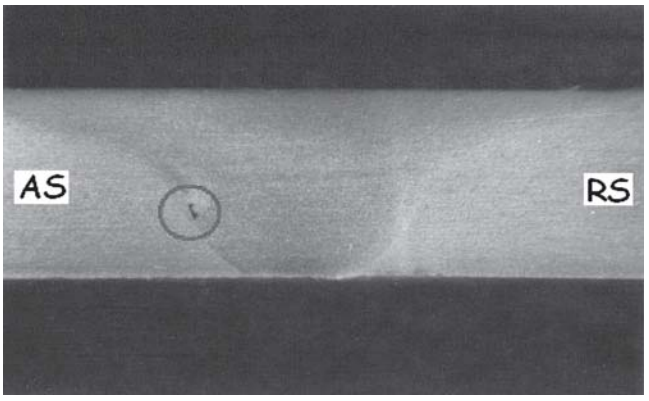

Fig. 12 Welding defect on the advancing side of the weld line in experiments (Ref 2)

4.5.3 Over XZ-Plane. As shown in Fig. 16 for the top view and bottom view of the distribution of the effective strain, there was little variation of strains in the thickness direction.

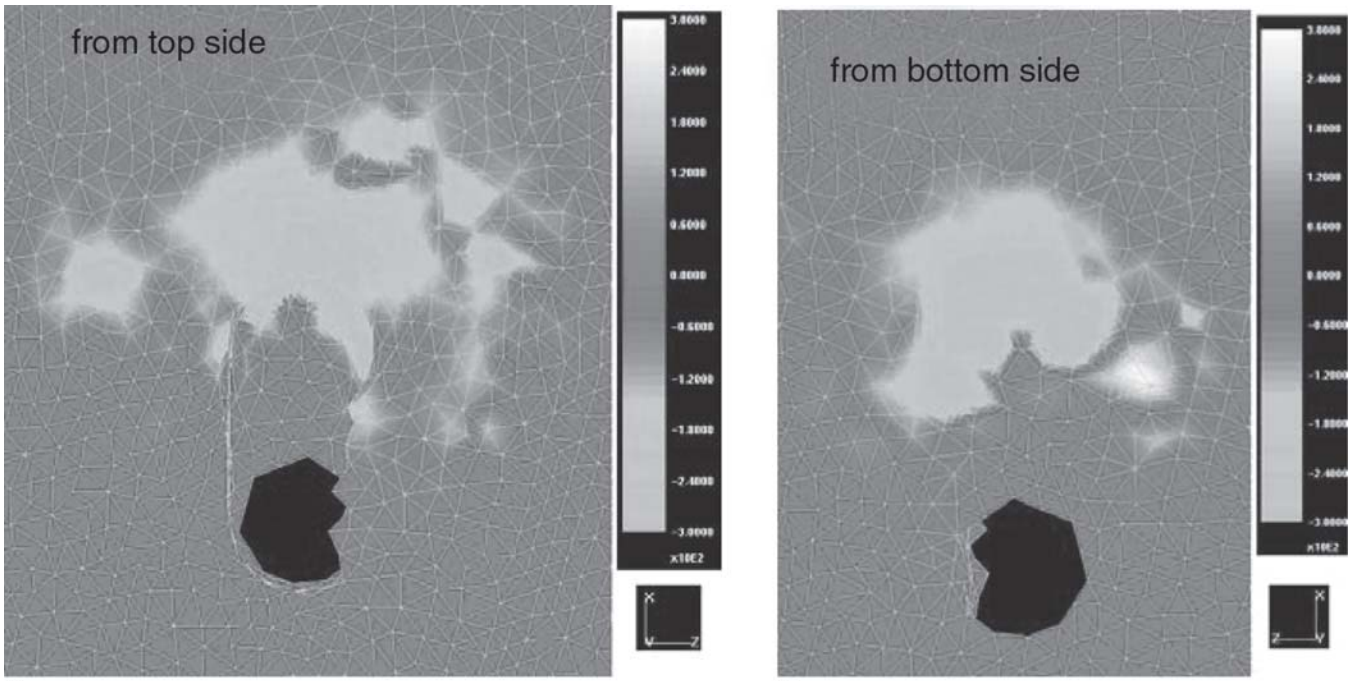

Fig. 13 Distribution of the mean stresses over the XZ-plane

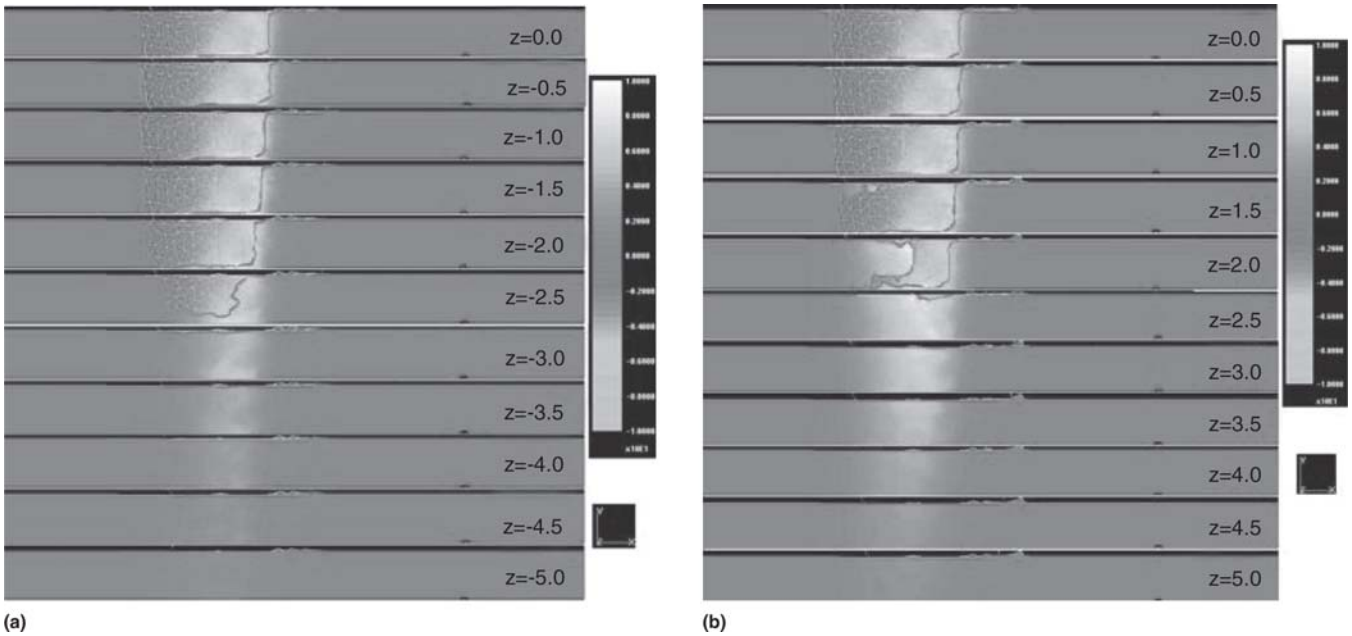

Fig. 14 Distribution of the effective strain over the XY-plane toward the (a) advancing and (b) retreating sides

4.6 Distribution of Effective Strain-Rates (Range 0 to 10 s)

4.6.1 Over XY-Plane. As shown in Fig. 17(a) (toward the advancing side) and Fig. 17(b) (toward the trailing side), there was little difference in the distribution of the effective strain rates, which are mostly concentrated at the contact interface between the pin and plate material. The extent of the distribution of effective strain rates in the lateral direction was very low (i.e., the gradient is very high).

4.6.2 Over YZ-Plane. As represented by Fig. 18(a) (toward the advancing side) and Fig. 18(b) (toward the trailing side), it was observed again that the extent of the distribution of effective strain rates was lower, and was concentrated at the contact interface between the pin and plate material.

4.6.3 Over XZ-Plane. As depicted in Fig. 19(a), which shows the distribution of effective strain rates on the left-half/advancing side and the full surface, it is evident that strain rates are concentrated at the contact interface and mostly toward the advancing side of the weld line. There was noticeable but little difference between the distributions of strain rates at the top surface (Fig. 19a) and the bottom surface of the plate (Fig. 19b).

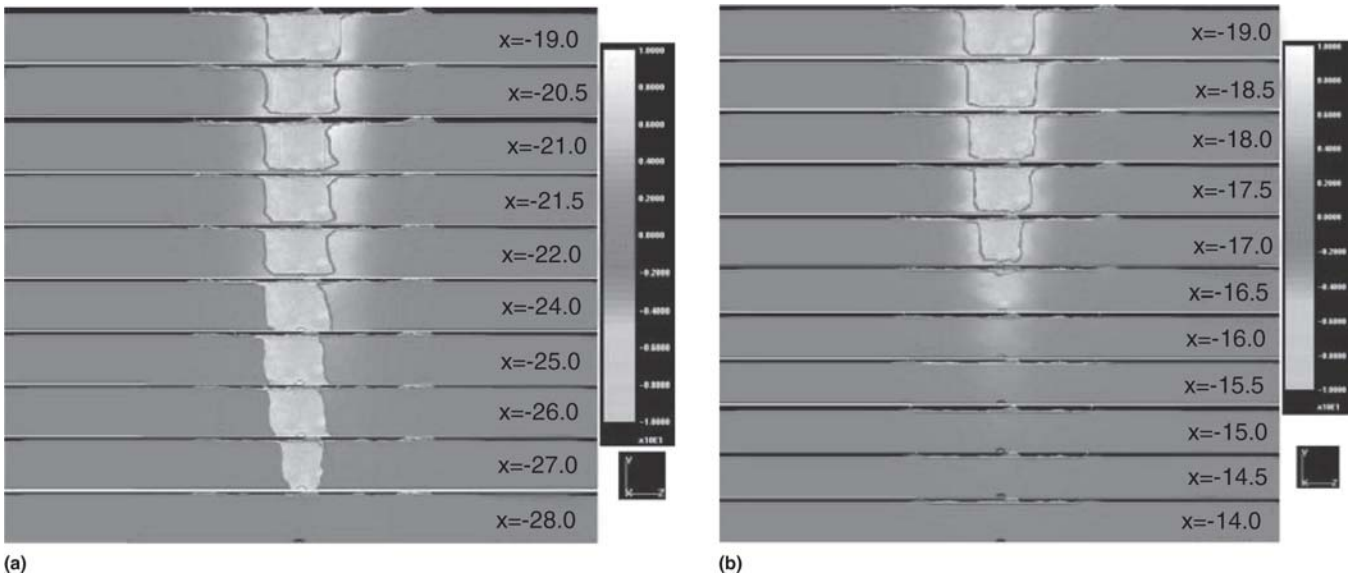

Fig. 15 Effective strain distribution over the YZ-plane toward the (a) trailing and (b) leading edge

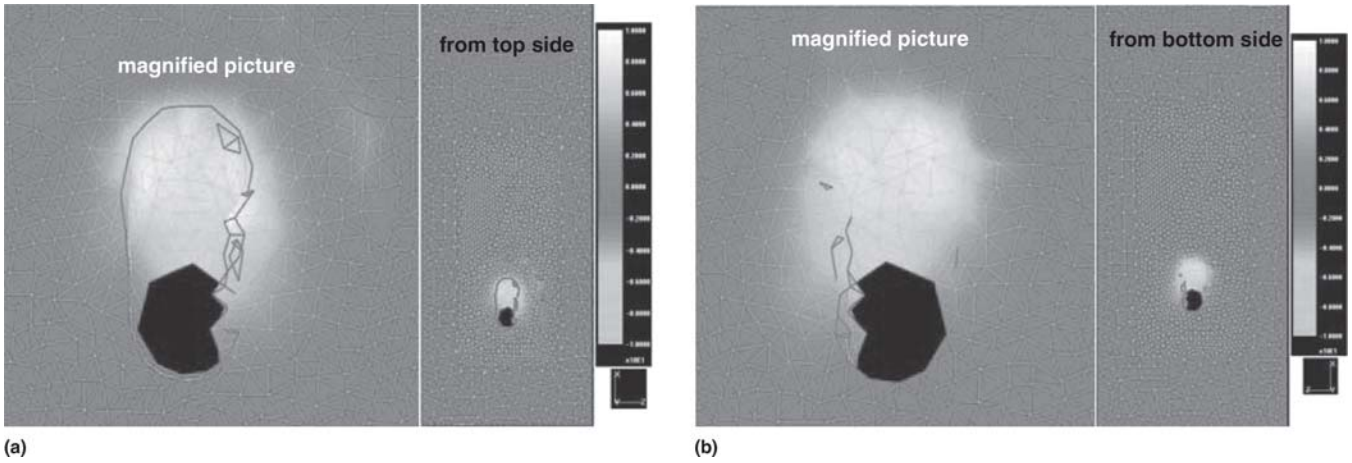

Fig. 16 Distribution of the effective strains over the (a) top and (b) bottom surfaces of the plate

5. Discussion

The variation of different critical process parameters was depicted using the figures cited in the previous section. The distribution of these parameters could be summarized as follows: temperature distribution is well beyond the contact surfaces, gradually diminishing away from tool center; effective stresses exists all over the plate, but are concentrated at the interface of the tool and plate; the mean stress distribution is confined to the contact area between the tool and pin; and the nature of these stresses changes from compressive to tensile where the presence of tensile stresses might lead to welding defects; and the distributions of effective strains and effective strain rates are mainly confined to the contact interface between the pin portion of the tool and the plate.

As depicted by the temperature distribution profiles (Fig. 3-5), it was evident that high temperatures are concentrated at the contact interface between the tool and plate toward the leading edge/retreating side of the pin. While welding similar material workpieces, this temperature variation might lead to differences in microstructure, which in turn lessens the service life of the component. On the other hand, this temperature variation could be beneficial while welding dissimilar materials, where material with a high melting point could be placed on the retreating side of the tool. A symmetric temperature distribution can be achieved by distributing the friction heat generated at the interface between the tool and plate. This can be attained by tilting the tool toward the low-temperature regions.

Concentrated effective stresses are believed to be caused by temperature gradients and the action of shear forces as a result of tool rotation. These results are similar to the results obtained by Chen and Kovacevic (Ref 28, 29), who simulated FSW with the use of the FE package ANSYS.

From the distributions of mean stresses, as shown in Fig. 10, 11, and 13, it is possible to predict the occurrence of welding defects because tensile mean stresses cause the nucleation of cracks. Simulation results gave a good prediction of the sites where tensile mean stresses exists, thus indicating probable sites for the nucleation of cracks. It can be concluded that

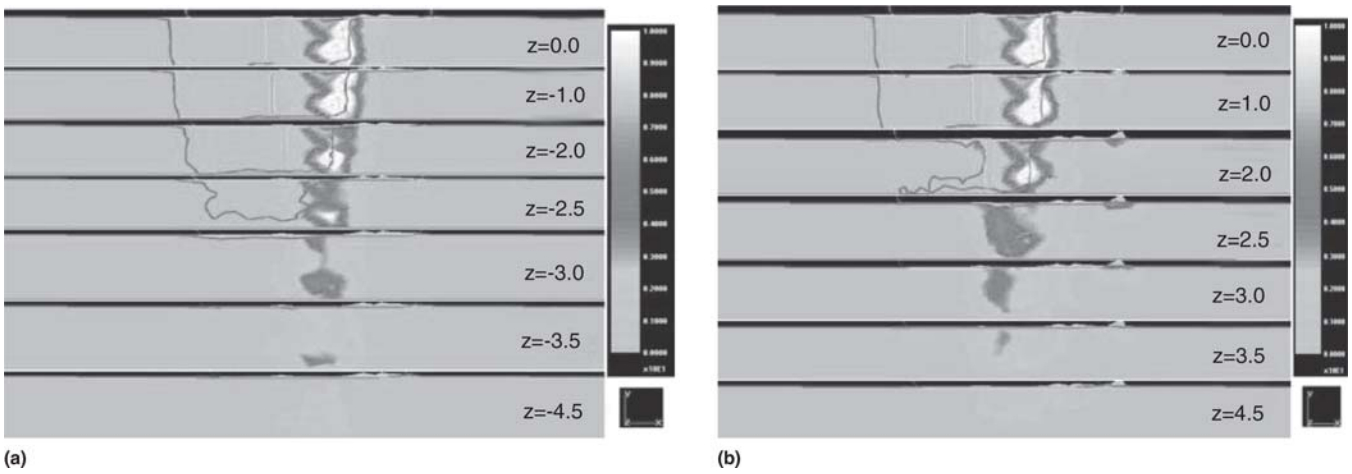

Fig. 17 Effective strain distribution over the XY-plane toward the (a) advancing and (b) retreating sides

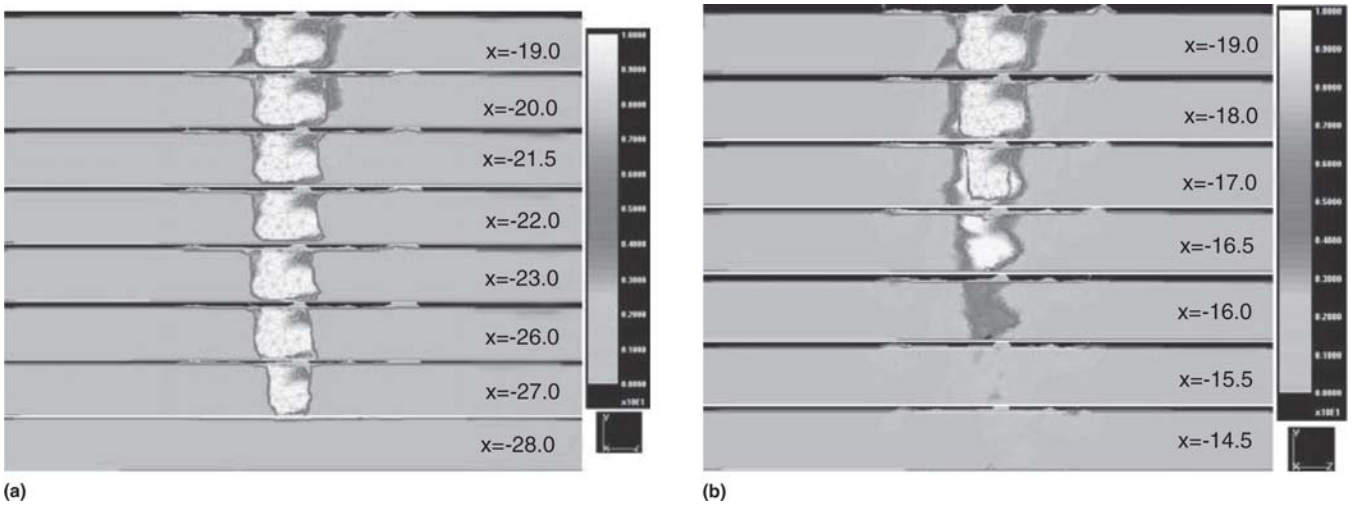

Fig. 18 Distribution of the effective strain rates over the YZ-plane toward the (a) trailing and (b) leading edge side

modeling using DEFORM can reasonably simulate the FSW process.

The distributions of effective strains and effective strain rates along with other parameters show that there exist very high gradients toward the advancing side of the weld line compared with the distribution toward the retreating side. This can be an indication of the presence of a sharp interface on the advancing side from a microstructural point of view. The presence of a sharp interface on the advancing side can be seen in experiments, while the interface at the retreating side is diffusive, as shown in Fig. 20.

6. Further Study Planned

As observed in many of the above figures, the initial hole that was made in which to insert the pin was not filled properly. Some material was observed to splash over the top surface of the plate. This might be due to the relatively larger size of the elements used in the FE simulation. Material has to extrude through a narrow gap between the pin and the plate, and the process simulation might be able to predict the filling of the hole if very small elements are used. That can considerably increase the simulation time. Once the simulation with a very fine mesh is able to deliver good results, a simulation of the whole process can be planned.

The point tracking option might give a graphical representation of the critical variables discussed in the previous sections, especially as a function of time and/or distance. Authors are not able to exercise this option due to the lack of complete filling during the welding process.

Further simulations can be planned to study the feasibility of welding dissimilar materials by tilting the tool in appropriate directions, as performed by Ulysse (Ref 46). In addition, the study of different pin profiles and different contact shapes of interfaces between shoulder and plate can give a better understanding of the FSW needed to attain the required weld quality.

Companies continue to develop advanced software for increasingly less expense. At the same time, extensive and widespread research is being performed to develop new applications. All applications require not only a deep understanding of the physics, but data on material properties under different environments (e.g., varying temperature and very high strain rates). This information is often not available or is incomplete. Work is being carried out to determine the values for these properties to make the models more accurate.

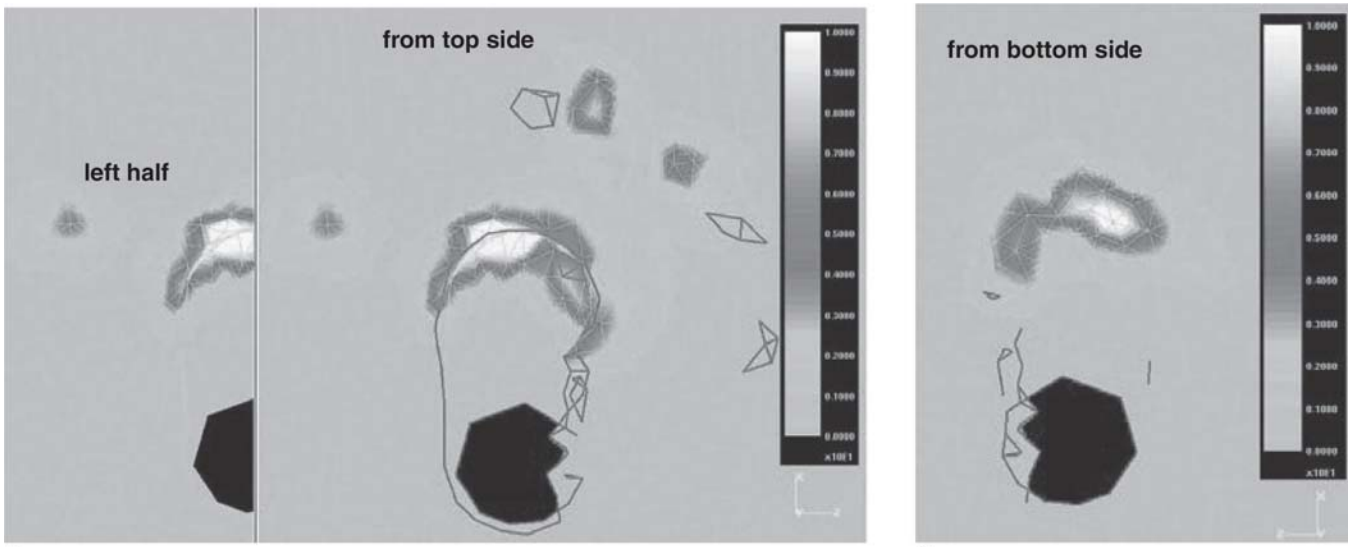

Fig. 19 Distribution of the effective strain rates on the XZ-plane

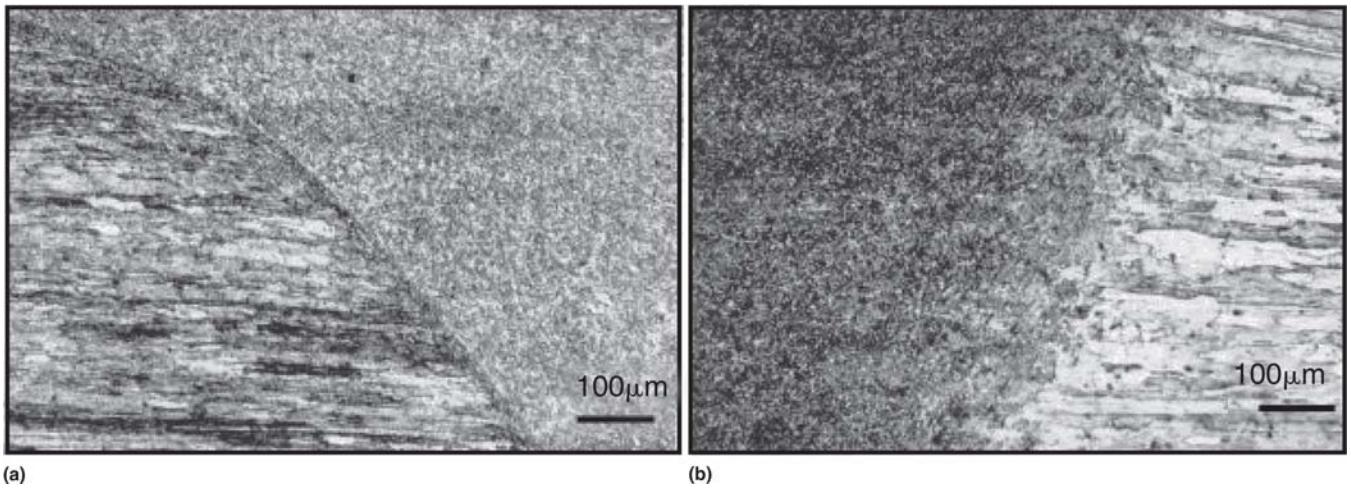

Fig. 20 Presence of a sharp interface and diffusive interfaces, respectively, on the (a) advancing side and (b) retreating side (Ref 2)

To understand and accurately model the mechanical response of welds, it is critical to have constitutive data for the various microstructural regions that make up the weld (e.g., the fusion zone or the dynamically recrystallized zone in FSW), the heat-affected zone, and the base metal.

7. Concluding Remarks

The commercially available 3-D finite-element code DEFORM has been used to demonstrate the distribution of process parameters during FSW to a reasonable extent. Based on the numerical results, the following conclusions can be drawn:

- Further studies of FSW are required for better process simulation of the complete welding operation using DEFORM.
- Many of the process parameters have a high gradient toward the leading edge of the tool, the advancing side of the weld line, or both. Experimental results confirm these trends due to the presence of a sharp interface on the advancing side and a diffusive interface on the retreating side.
- The maximum temperature recorded is about 350 °C, which is less than expected. Changes in thermal properties and heat transfer parameters could improve the simulation results.
- The DEFORM simulations are able to locate the sites for the probable presence of welding defects in terms of tensile mean stresses. Again, experimental results augment these simulation results.
- The distribution of temperatures could be altered by tilting the tool in appropriate directions to weld dissimilar metals or to attain a symmetric temperature profile over the weld line in the welding of similar materials.

References

1. K. Kumar and V.S. Kailas, "Friction Stir Welding," presented at International Congress on Sheet Metal Forming Technology for Global Competitiveness (New Delhi, India), 2004
2. K. Kumar and V.S. Kailas, "Influence of Tool Geometry on Defect Formation, Microstructure and Mechanical Properties of a Friction Stir Welded Aluminium Alloy," presented at the Second International Conference on Advances in Production and Processing of Aluminium APPA 2005 Proceedings (Bahrain), December 2005, University of Bahrain, p III-8-1-12
3. K. Kumar and V.S. Kailas, "On the Role of Axial Load and the interface Position on the Strength of a Friction Stir Welded Aluminium Alloy," presented at the second international conference on Advances in Production and Processing of Aluminium APPA 2005 proceedings (Bahrain), December 2005, University of Bahrain, p III-9-1-11
4. G. Campbell and T. Stotler, Friction Stir Welding of Armor Grade Aluminum Plate, *Weld. J.,* 1999, **78**(12), p 45-48
5. Y.J. Chao and X. Qi, Thermal and Thermo-Mechanical Modeling of Friction Stir Welding of Aluminum Alloy 6061-T6, *J. Mater. Manufact. Sci.,* 1999, **7**(2), p 215-233
6. K. Colligan, Material Flow Behavior During Friction Stir Welding of Aluminum, *Weld. J.,* 1999, **78**(7), p 229-237
7. P. Dong, F. Lu, J.K. Hong, and Z. Cao, "Analysis of Weld Formation Process in Friction Stir Welding," presented at the 1st International Symposium on Friction Stir Welding (Thousand Oaks, CA), June 1999
8. O.V. Flores, C. Kennedy, L.E. Murr, D. Brown, S. Pappu, B.M. Nowak, and J.C. McLure, Microstructural Issues in a Friction Stir Welded Aluminum Alloy, *Scripta Mater.,* 1998, **38**(5), p 703-708
9. Ø. Frigaard, Ø. Grong, B. Bjorneklett, and O.T. Midling, "Modelling of the Thermal and Microstructural Fields During Friction Stir Welding of Aluminium Alloys," presented at the 1st International Symposium on Friction Stir Welding (Thousand Oaks, CA), June 1999
10. J.E. Gould and Z. Feng, Heat Flow Model for Friction Stir Welding of Aluminum Alloys, *J. Mater. Manufact. Sci.,* 1999, **7**(2), p 185-194
11. G. Liu, L.E. Murr, C.S. Niou, J.C. McLure, and F.R. Vega, Microstructural Aspects of the Friction Stir Welding of 6061-T6 Aluminum, *Scripta Mater.,* 1997, **37**(3), p 355-361
12. L.E. Murr, G. Liu, and J.C. McLure, Dynamic Recrystallization in Friction-Stir Welding of Aluminum Alloy 1100, *J. Mater. Sci. Lett.,* 1997, **16,** p 1801-1803
13. A.P. Reynolds and W.D. Lockwood, "Digital image Correlation for Determination of Weld and Base Metal Constitutive Behavior," presented at the 1st International Symposium on Friction Stir Welding (Thousand Oaks, CA), June 1999
14. A.P. Reynolds, T.U. Seidel, and M. Simonsen, "Visualization of Material Flow in an Autogenous Friction Stir Weld," presented at the 1st International Symposium on Friction Stir Welding (Thousand Oaks, CA), June 1999
15. C.G. Rhodes, M.W. Mahoney, W.H. Bingel, R.A. Spurling, and C.C. Bampton, Effects of Friction Stir Welding on Microstructure of 7075 Aluminum, *Scripta Mater.,* 1997, **36**(1), p 69-75
16. W. Tang, X. Guo, J.C. McClure, L.E. Murr, and J.Q. Sun, Heat Input and Temperature Distribution in Friction Stir Welding, *J. Mater. Manufact. Sci.,* 1999, **7**(2), p 163-172
17. M.Z.H. Khandkar and J.A. Khan, Thermal Modeling of Overlap Friction Stir Welding for Al-Alloys, *J. Mater. Process. Manuf. Sci.,* 2001, **10,** p 91-105
18. R.W. Fonda and S.G. Lambrakos, Analysis of Friction Stir Welds Using an Inverse Problem Approach, *Sci. Technol. Welding Joining,* 2002, **7**(3), p 177-181
19. R.W. Fonda, J.F. Bingert, and K.J. Colligan, Development of Grain Structure During Friction Stir Welding, *Scripta Mater.,* 2004, **51,** p 243-248
20. M.G. Dawes, S.A. Karger, T.L. Dickerson, and J. Przydatek, "Strength and Fracture Toughness of Friction Stir Welds in Aluminum Alloys," presented at the 2nd International Symposium on Friction Stir Welding (Gothenburg, Sweden), June 2000
21. L. Cederqvist and A.P. Reynolds, "Properties of Friction Stir Welded Aluminum Lap Joints," presented at the 2nd International Symposium on Friction Stir Welding (Gothenburg, Sweden), June 2000
22. L. Magnusson and L. Källman, "Mechanical Properties of Friction Stir Welds in Thin Sheet of Aluminium 2024, 6013 and 7475," presented at the 2nd International Symposium on Friction Stir Welding (Gothenburg, Sweden), June 2000
23. D.J. Kinchen, Z. Li, and G.P. Adams, "Mechanical Properties of Friction Stir Welds in Al-Li 2195-T8," presented at the 1st International Symposium on Friction Stir Welding (Thousand Oaks, CA), June 1999
24. T. Hashimoto, S. Jyogan, K. Nakata, Y.G. Kim, and M. Ushio, "FSW Joints of High Strength Aluminum Alloy," presented at the 1st International Symposium on Friction Stir Welding (Thousand Oaks, CA), June 1999
25. J.C. Bassett and S.S. Birley, "Friction Stir Welding of Aluminium Armour," presented at the 2nd International Symposium on Friction Stir Welding (Gothenburg, Sweden), June 2000
26. www.mts.com/aesd/friction_stir.htm
27. M. Skinner and R.L. Edwards, Improvements to the FSW Process Using the Self-Reacting Technology, *Mater. Sci. Forum,* 2003, **426-432,** p 2849-2854
28. C.M. Chen and R. Kovacevic, Prediction of Evolutional Stress in Friction Stir Welding, *Proceedings of Materials Science and Technology 2003 Meeting,* 2003, Chicago, TMS, p 357-368
29. C.M. Chen and R. Kovacevic, Finite Element Modeling of Friction Stir Welding: Thermal and Thermo-Mechanical Analysis, *Int. J. Machine Tools Manufact.,* 2003, **43,** p 1319-1326
30. M. Song and R. Kovacevic, Numerical and Experimental Study of the Heat Transfer Process in Friction Stir Welding, *J. Eng. Manufact., B,* 2003, **217,** p 73-85
31. M. Song, R. Kovacevic, J. Ouyang, and M. Valant, "A Detailed Three-Dimensional Transient Heat Transfer Model for Friction Stir Welding," presented at ASM Proceedings of the International Conference: Trends in Welding Research, ASM International, 2002, p 212-217
32. M. Song and R. Kovacevic, Thermal Modeling of Friction Stir Welding in a Moving Coordinate System and Its Validation, *Int. J. Machine Tools Manufact.,* 2003, **43,** p 605-615
33. Y. Cao and X. Qi, Thermal and Thermo-Mechanical Modeling of Friction Stir Welding of Aluminum Alloy 6001-T6, *J. Mater. Proc. Manufact. Sci.,* 1998, **7**(10), p 215-233
34. G. Oertelt, S.S. Babu, S.A. David, and E.A. Kenik, Effect of Thermal Cycling on Friction Stir Welds of 2195 Aluminum Alloy, Weld. Res., 2001, **80**(3), (suppl), p 71-79
35. H. Schmidt, J. Hattel, and J. Wert, An Analytical Model for the Heat Generation in Friction Stir Welding, *Model. Simul. Mater. Sci. Eng.,* 2004, **12,** p 143-157
36. M.Z.H. Khandkar and J.A. Khan, Thermal Modeling of Overlap Friction Stir Welding for Al-Alloys, *J. Mater. Proc. Manuf. Sci.,* 2001, **10,** p 91-105
37. M.Z.H. Khandkar, J.A. Khan, and A.P. Reynolds, "A Thermal Model of the Friction Stir Welding Process," presented at proceedings of the 6th International Conference on Trends in Welding Research, ASM International, 2002, p 218-223
38. M.Z.H. Khandkar and J.A. Khan, Predicting Residual Thermal Stresses in Friction Stir Welding, *American Society of Mechanical Engineers, Heat Transfer Division, (Publication), HTD,* 2003, **374**(3), p 355-360
39. A. Steuwer, M. Peel, P.J. Withers, T. Dickerson, Q. Shi, and H.R. Shercliff, Measurement and Prediction of Residual Stresses in Aluminium Friction Stir Welds, *J. Neutron Res.,* 2003, **11**(4), p 267-272
40. D. Lawrjaniec, A. Abisror, C. Decker, M. Kocak, and J. Dos Santos, Numerical Simulation of Friction Stir Welding, *Mater. Sci. Forum,* 2003, **426-432,** p 2993-2998
41. L. Tianzhong, T.U. Seidel, T. Wei, and A.P. Reynolds, "A Friction Stir Welding Model Using Computational Fluid Dynamics," presented at *Hot Deformation of Aluminum Alloys III, 2003 TMS Annual Meeting,* The Materials Society, 2003, p 299-312
42. P. Heutier, M.J. Jones, C. Desrayaud, J.H. Driver, and F. Montheillet, Thermomechanical Conditions and Resultant Microstructures in Friction Stir Welded 2024 Aluminium, *Mater. Sci. Forum,* 2003, **426-432,** p 2927-2932
43. A.P. Reynolds, K. Linder, W. Tang, and T.U. Seidel, Weld Efficiency and Defect Formation: Correlation Between Experiment and Simple Models, *ASM Proceedings of the International Conference: Trends in Welding Research,* ASM International, 2002, p 297-301
44. H.N. Schmidt, J. Hattel, and J.R. Wert, Modeling of the Contact Condition at the Tool/Matrix Interface In Friction Stir Welding, *7th International Seminar on Numerical Analysis Of Weldability, Mathematical Modeling of Weld Phenomena,* Vol 7, H. Cerjak and H.K.D.H. Bhadeshia, Ed., TMS, p 12
45. A. Askari, S. Silling, B. London, and M. Mahoney, Modeling and Analysis of Friction Stir Welding Processes, *Proceedings of Symposium on Friction Stir Welding and Processing,* November 4–8, 2001 (Indianapolis, IN), TMS, p 43-54

46. P. Ulysse, Three-Dimensional Modeling of the Friction Stir-Welding Process, *Int. J. Machine Tools Manufact.,* 2002, **42,** p 1549-1557
47. X.K. Zhu and Y.J. Chao, Numerical Simulation of Transient Temperature and Residual Stresses in Friction Stir Welding of 304L Steel, *J. Mater. Process. Technol.,* 2004, **146,** p 263-272
48. G. Aramayo, B. Radhakrishanan, S.A. David, G. Sarma, and S.S. Babu, "Modeling of Friction Stir Welding Process for Fusion Energy Applications," Oak Ridge National Laboratory
49. W.D. Lockwood, B. Tomaz, and A.P. Reynolds, Mechanical Response of Friction Stir Welded AA2024: Experiment and Modeling, *Mater. Sci. Eng., A,* 2002, **323,** p 348-353
50. W.D. Lockwood and A.P. Reynolds, Simulation of the Global Response of a Friction Stir Weld Using Local Constitutive Behavior, *Mater. Sci. Eng., A,* 2003, **339,** p 35-42
51. G. Buffa and L. Fratini, Friction Stir Welding of AA6082-T6 Sheets: Numerical Analysis and Experimental Tests, *Proceedings of NUMIFORM 2004, Materials Processing and Design: Modelling, Simulation, and Applications,* p 1224–1229
52. L. Fratini and G. Buffa, CDRX Modelling in Friction Stir Welding of Aluminium Alloys, *Int. J. Machine Tools Manufact.,* 2005, **45,** p 1188-1194
53. J.H. Ouyang and R. Kovacevic, Material Flow and Microstructure in the Friction Stir Butt Welds of the Same and Dissimilar Aluminium Alloys, *J. Mater. Eng. Perf.,* 2002, **11,** p 51-63
54. M. Guerra, C. Schmidt, J.C. McClure, L.E. Murr, and A.C. Nunes, Flow Patterns During Friction Stir Welding, *Mater. Charact.,* 2003, **49,** p 95-101
55. L.E. Murr, R.D. Flores, O.V. Flores, J.C. McClure, G. Liu, and D. Brown, Friction Stir Welding: Micro-Structural Characterization, *Mater. Res. Innov.,* 1998, **1,** p 211-223
56. L.E. Murr, Y. Li, R.D. Flores, E.A. Trillo, and J.C. McClure, Intercalation Vortices and Related Micro-Structural Features I the Friction Stir Welding of Dissimilar Metals, *Mater. Res. Innov.,* 1998, **2,** p 150-163
57. Y. Li, L.E. Murr, and J.C. McClure, Flow Visualization and Residual Microstructures Associated with the Friction Stir Welding of 2024 Aluminium to 6061 Aluminium, *Mater. Sci. Eng., A,* 1999, **271,** p 213-223
58. Y. Li, L.E. Murr, and J.C. McClure, Solid-State Flow Visualization in the Friction Stir Welding of 2024 Al to 6061 Al, *Scripta Mater.,* 1999, **40,** p 1041-1046
59. A.P. Reynolds, Visualization of Material Flow in Autogeneous Friction Stir Welds, *Sci. Technol. Weld. Join.,* 2000, **5,** p 120-124
60. K. Colligan, Material Flow Behavior During Friction Stir Welding of Aluminium, *Weld. J.,* 1999, **78**(7), p 229-237
61. K.N. Krishnan, On the Formation of Onion Rings in Friction Stir Welds, *Mater. Sci. Eng., A,* 2002, **327,** p 246-251
62. J.A. William, Modeling Friction Stir Joining as a Metal Working Process, TMS Annual Meeting 2003, The Materials Society, p 313–327
63. www.deform.com.